Accurate Multi-Ended Fault Locating Algorithm Using Incremental Sequence Quantities

Arun Shrestha and Sathish Kumar Mutha, *Schweitzer Engineering Laboratories, Inc.*

***Abstract*—Accurate fault location of transmission line faults allows crews to make necessary repairs to quickly restore power. A new multi-ended fault location algorithm that uses pure-fault networks and incremental sequence quantities is presented in this paper. The proposed method uses time-synchronized voltage and current samples from all remote terminals, which makes this method suitable for integration in line current differential relays. Compared with the traditional multi-ended fault location method that solves faulted networks, this method provides better fault location estimates for untransposed lines. This paper demonstrates the accuracy of the proposed pure-fault network method by using simulations and field cases.**

I. Introduction

Protective relays detect faults on the transmission lines and circuit breakers isolate them from the power system. Following a fault, fault locator functions available on the protective relays or standalone fault locators provide critical information about the fault, such as fault type and fault location. Accurate fault location allows utility crews to quickly locate the faulty equipment, make necessary repairs, and restore power. This leads to reduced outage time, revenue loss, and end-user complaints. The importance of accurate fault location is highlighted for transmission systems constructed over rough terrain and when service needs to be restored during severe weather conditions. Precise fault location is critical for expedited service restoration and improving power system reliability, and it is valuable to power system operators and transmission asset owners.

Fault location techniques for transmission lines can be broadly classified into traveling-wave-based and impedance-based methods. Traveling-wave fault location (TWFL) algorithms use the arrival times of fault-generated traveling waves, line length, and line propagation time to estimate fault location. TWFL methods provide better accuracy than impedance-based fault location methods, which use fundamental frequency voltage, current phasors, and transmission line parameters to estimate fault location.

Impedance-based fault locating can be further classified into single-ended and multi-ended impedance-based techniques. In the single-ended technique, voltage and current phasors from only one end of the transmission line are used. The multi-ended fault location technique uses either only remote terminal currents or both remote terminal voltages and currents. The multi-ended fault location method is typically used in line current differential relays. When both remote terminal voltages and currents are used in the multi-ended fault location method, the fault location accuracy is not impacted by system non-homogeneity or fault resistance. Also, this method is independent of transmission line zero-sequence impedance.

To analyze faults on a transmission line in a complex network, the overall network can be simplified into a two-source power system connected by the transmission line of interest using Thevenin's theorem. Furthermore, the principle of superposition can be used to represent any faulted network as a summation of two separate networks [1]: a pre-fault network and a pure-fault network. Incremental quantities contain only fault-induced signals that appear in the pure-fault network. These quantities are typically represented with the delta prefix (Δ) to indicate the change, with respect to the pre-fault network signals. Relays measure both the pre-fault and faulted-network signals directly.

This paper describes a new multi-ended fault location algorithm using pure-fault networks and incremental sequence quantities. The proposed method uses time-synchronized voltages and currents from both local and remote terminals. All calculations are performed using phasor data. Following a fault, the proposed algorithm stores pre-fault and fault phasors. Next, incremental negative-sequence and positive-sequence phasors are calculated by subtracting pre-fault from fault sequence quantities. For unbalanced faults, pure-fault negative-sequence network is solved using incremental negative-sequence phasors from all terminals to estimate the fault location. Similarly, fault location for a three-phase fault is estimated by solving pure-fault positive-sequence network using incremental positive-sequence phasors. The proposed pure-fault network method does not require dedicated fault-type identification logic for unbalanced faults and uses two equations to estimate fault location for all ten fault types. The use of incremental sequence quantities eliminates the impact of pre-fault system unbalance in the fault location estimation. Compared with the multi-ended fault location method that solves using a faulted network, this method provides better fault location estimates for untransposed lines. This paper demonstrates the accuracy of the proposed method by using simulations and field data. The results from two- and three-terminal lines are included in this paper.

II. Fault Location Methods

Fault location methods can be broadly classified into two groups:

- Traveling-wave methods
  - Type A, B, C, D, and E
- Impedance-based methods
  - Single-ended
  - Multi-ended

A. Traveling-Wave Methods

When a fault occurs at the point on the voltage wave other than the zero-voltage point, high-frequency step waves are launched. These step waves, also known as traveling waves, are launched from the fault point and propagate away from the fault point in both directions towards the terminals. Traveling waves on overhead transmission lines travel at velocities close to the speed of light. Traveling-wave fault locators estimate very accurate fault location by detecting these waves and using the arrival times of incident and reflected waves.

There are five distinct TWFL methods. These techniques are referred to as Type A, B, C, D, and E respectively [2]. Single-ended (Type A) and double-ended (Type D) are the two commonly used methods in traveling-wave fault locators. In the single-ended traveling-wave method, the fault locator estimates the fault location by using the time difference between the first arrived wave and the successive reflected wave from the fault point. This method does not require any protection signaling channel or any data from the remote end. This method requires processing of subsequent traveling-wave reflection and poses some challenges using current-based traveling waves. The double-ended traveling-wave method estimates the first traveling-wave arrival times at both ends of a transmission line and uses the time difference for fault location estimation. Because reflected waves are not used, algorithm implementation is simplified. This method requires a precise time stamp of the first traveling wave from the remote device.

Traveling-wave methods require accurate line length measurements, traveling-wave propagation velocity, and precise time stamp information. Because these methods do not use line positive- and zero-sequence impedance data, errors in line impedance have no impact on TWFL. Propagation velocity is usually calculated from line energization tests or from external fault event reports [3]. In real-world fault events, traveling-wave methods have provided accuracies as low as 300 meters, or about one tower span [4] [5].

B. Impedance-Based Methods

Impedance-based fault location methods use fundamental frequency voltages and currents captured by protective relays or fault locators to estimate fault location. In the single-ended method, the fault locator estimates the fault location from the apparent impedance between the device and the fault. This method is simple to implement and does not require any communications. Six fault loops are solved to cover all fault types. The fault location accuracy for the single-ended method depends on the fault resistance; system non-homogeneity; inaccuracy of line parameters, particularly zero-sequence impedance; zero-sequence mutual coupling; incorrect fault-type identification; and load flow unbalance [2] [6]. To limit fault location error due to fault resistance and load current, different algorithms are implemented within the single-ended method. Single reactance method, Takagi method, Modified Takagi method, and Current Distribution Factor method all fall under singled-ended fault location technique [2].

In the multi-ended fault location method, either only remote terminal currents or both remote terminal voltages and currents are used. Furthermore, algorithms are available to estimate fault location using either unsynchronized or synchronized remote terminal data [2] [7]. Line current differential relays usually include a multi-ended method that uses synchronized local and remote signals. The fault location accuracy is not impacted by fault resistance and system non-homogeneity. When both remote voltages and currents are used, inaccuracies in line zero-sequence impedance and zero-sequence mutual coupling do not influence accuracy. Multi-ended methods have been developed to accurately estimate fault location on three- and four-terminal lines [8].

III. Untransposed Lines and Their Impact On Multi-Ended Fault Location Accuracy

Transposition is the technique of rotating the positions of a transmission line's phases at intervals to ensure that each phase in turn occupies all positions in each line configuration [2]. When transmission lines are transposed, it equalizes the mutual inductances between the phases. In practice, lines are often constructed without transpositions to keep the construction cost down [9]. Faults are also more likely to occur at transpositions [10]. Untransposed lines create unbalance in the network, which in turn generates negative- and zero-sequence voltages and currents. The unbalance is considerable for long untransposed lines with heavy load flow. The negative- and zero-sequence quantities generated by untransposed lines impact protection algorithms and fault location methods.

Adverse impacts of voltage unbalance on generation, transmission, distribution, and end-user equipment for a utility is documented in [11]. The utility experienced voltage unbalance levels increasing over a period of several years. Following a study, the utility concluded that untransposed 500 kV transmission lines are the key contributor to voltage unbalance in their system. The study also found the direct correlation between voltage unbalance and transmission line loadings. As a remedial action, costly line transposition projects were carried out for three 500 kV lines. Following the line transposition, the voltage unbalance issue was significantly improved.

Table V in the Appendix shows the line parameters and tower configuration for a 400 kV overhead transmission line. For the given line, resistance, inductance, capacitance (RLC) matrices at 60 Hz are listed in (12). The impedance (Z_{ABC}) and symmetrical component (Z_{012}) matrix for a 100 km untransposed 400 kV line are shown in (1) and (2).

$$Z_{ABC}(\Omega)=\begin{pmatrix}11.20+52.54i & 9.84+20.09i & 9.45+15.42i\\ 9.84+20.09i & 11.50+51.78i & 9.84+20.09i\\ 9.45+15.42i & 9.84+20.09i & 11.20+52.54i\end{pmatrix} \quad (1)$$

$$Z_{012}(\Omega)=\begin{pmatrix}30.74+89.36i & 1.01-0.84i & -1.24-0.45i\\ -1.24-0.45i & 1.58+33.75i & -2.83+1.82i\\ 1.01-0.85i & 2.99+1.54i & 1.58+33.75i\end{pmatrix} \quad (2)$$

Because of the unequal distance between phases, the mutual impedances are unequal in the Z_{ABC} matrix. Similarly, off-diagonal terms are not zero in the symmetrical component matrix, Z_{012}. When developing sequence networks, we assume the power systems are symmetrical from the generators to the point of unbalance (fault or an open conductor). This results in the independence of the symmetrical components in a balanced system network. This means positive-sequence currents flowing in the balanced power system produce only positive-sequence voltage drops and no negative- and zero-sequence drops. The same is true for negative- and zero-sequence current flow. With untransposed transmission lines, there is a coupling between the sequence networks. As a result, all three sequence voltages and currents appear in the pre-fault network. The magnitude of negative- and zero-sequence voltages and currents increases with the line loading [12]. The pre-fault unbalance directly impacts the fault location accuracy.

A. Impact on Fault Location Accuracy

To understand the impact of pre-fault unbalance generated by untransposed lines on fault location, tests are carried out on a simple two-source power system, as shown in Fig. 1. Line parameters from Table V in the Appendix are used for the transmission line. Both source voltages, E_S and E_R, are fixed to 1.0 pu. At first, the 400 kV transmission line is modeled as a fully transposed line. For this balanced system, A-phase-to-ground fault with a fault resistance of 10 ohms is applied at 30 km from the S-terminal. The left source, E_S, load angle is varied from –20° to 20° with a 1° increment between each fault, while the right source, E_R, angle is kept at 0°. For each fault, the fault location is estimated using the well-known double-ended impedance-based method shown in equation (3). Equation (4) is normally used for three-phase faults. Next, the transmission line is modeled as an untransposed line and the faults described earlier are applied again. Following the faults, fault location is estimated for an untransposed line model as well.

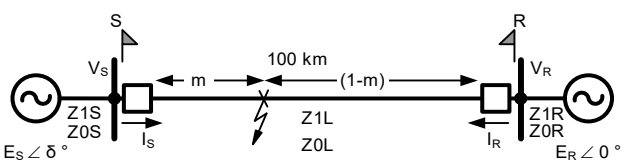

Fig. 1. Two-source power system model with single-circuit line.

$$m_{UNBALANCED\_FAULT}=\text{real}\left(\frac{V_{2S}-V_{2R}+Z_{1L}\bullet I_{2R}}{Z_{1L}\bullet(I_{2S}+I_{2R})}\right) \quad (3)$$

$$m_{BALANCED\_FAULT}=\text{real}\left(\frac{V_{1S}-V_{1R}+Z_{1L}\bullet I_{1R}}{Z_{1L}\bullet(I_{1S}+I_{1R})}\right) \quad (4)$$

The top and middle plots in Fig. 2 show pre-fault negative-sequence voltage and current magnitude measured at S and T terminals for both transposed and untransposed line models with respect to load angle δ. As expected, for transposed (TP) lines the pre-fault negative-sequence quantities are close to zero. However, there are reasonable pre-fault negative-sequence quantities for untransposed (UTP) line model. Fault location estimates for both line models with respect to load angle δ is shown in the bottom plot of Fig. 2. This plot shows the impact of pre-fault unbalance on double-ended impedance-based fault location method.

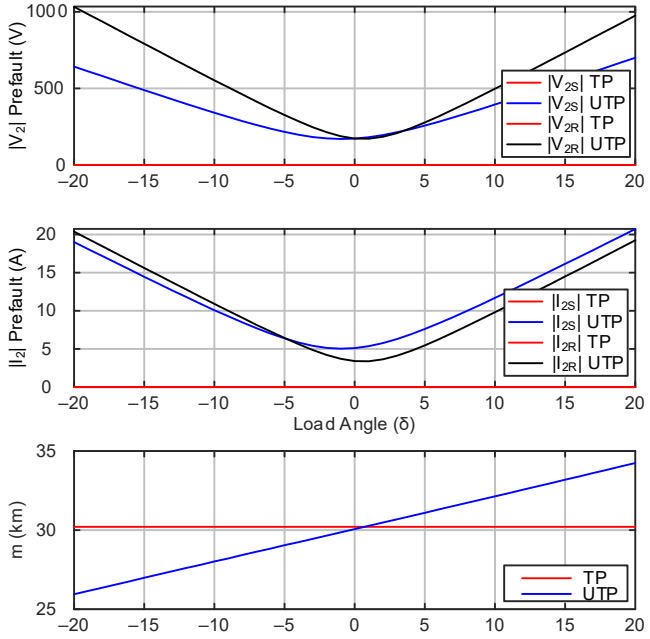

Fig. 2. Pre-fault |V2| and |I2| for both S and T terminals, and impedance-based fault location for transposed (TP) and untransposed (UTP) line models.

IV. Incremental Quantities

Thevenin's theorem and the principle of superposition can be used to represent any faulted network as a summation of two separate networks, a pre-fault network, and a pure-fault network. Fig. 3 shows these three networks for a fault on the line with fault resistance, R_F. The pre-fault network drives the load current through the network and establishes the voltage, V_F, at the fault location. All pre-fault network voltage sources are short-circuited in the pure-fault network, and the Thevenin source voltage that is equal to the negative pre-fault voltage at the fault location ($-V_F$) is included. The pure-fault network currents and voltages are zero before the fault. Pre-fault conditions and network parameters determine currents and voltages in the pure-fault network.

Incremental quantities, also referred to as superimposed quantities, are signals that appear in the pure-fault network [14] [13] [1]. These quantities are typically represented with the delta prefix (Δ) to indicate the change with respect to the pre-fault network signals. Because relays measure both the pre-fault and faulted-network signals, incremental quantities can be calculated by subtracting pre-fault network signals from

faulted-network signals. The incremental voltage and current quantities are expressed in (5).

$$\Delta V = V_{FAULTED} - V_{PRE\text{-}FAULT}$$
$$\Delta I = I_{FAULTED} - I_{PRE-FAULT} \quad (5)$$

Numerous protection algorithms have been developed by solving pure-fault networks either in the time-domain or in the frequency domain. In the time-domain, the relationship between incremental voltage and current quantities is governed by differential equations. In the frequency domain, phasors are used, and algebraic equations govern the relationship between incremental voltage and current phasors. When phasors are used, there is an inherent delay associated with the phasor filter required for accurate phasor estimation. This delay impacts the speed at which phasor-based incremental elements can operate.

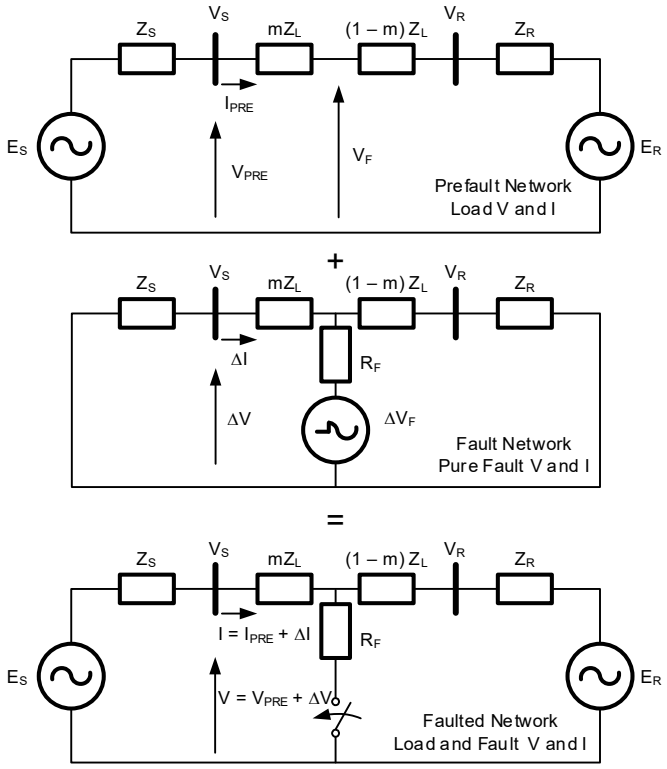

Fig. 3. Faulted network as the superposition of pre-fault network and pure-fault network [13].

In a balanced power network only positive-sequence current and voltage exist in the pre-fault network. For such a network, the calculated negative-sequence and zero-sequence quantities in the faulted network are incremental negative-sequence and zero-sequence quantities in the pure-fault network [15]. For such network, positive-sequence incremental quantities can be calculated by subtracting positive-sequence quantities between faulted and pre-fault networks.

As discussed in Section III, untransposed lines create unbalance and result in the generation of negative-sequence and zero-sequence voltages and currents in the pre-fault network. With unbalance in the pre-fault network, incremental negative-sequence and zero-sequence quantities in the pure-fault network are no longer the negative-sequence and zero-sequence quantities in the faulted network. These quantities impact the fault location accuracy.

V. Proposed Multi-Ended Fault Location Method

In Section III, we showed the impact that pre-fault unbalance due to untransposed lines has on fault location accuracy. In Section IV, we discussed that a faulted network is the summation of two separate networks, a pre-fault network and a pure-fault network. Using a pure-fault network and sequence incremental quantities that exist only in the pure-fault network, a new multi-ended impedance-based fault location method is proposed. Because we solve using a pure-fault network, the impact of pre-fault unbalance is eliminated and a much more accurate fault location is provided. The proposed method uses time-synchronized voltage and current samples from all remote terminals. Therefore, this method is suitable for integration in a line current differential relay that has access to remote voltage and current signals. Similarly, the proposed method can also be implemented in software that has access to time-stamped event reports.

Fig. 4 shows a simple two-source power system connected by a transmission line of interest. Each line relay measures the local line voltage and current signals. Using a communication channel, each relay exchanges the measured signals with the remote relay. The local and remote signals can be synchronized on each relay using an external time source or the well-known ping-pong method.

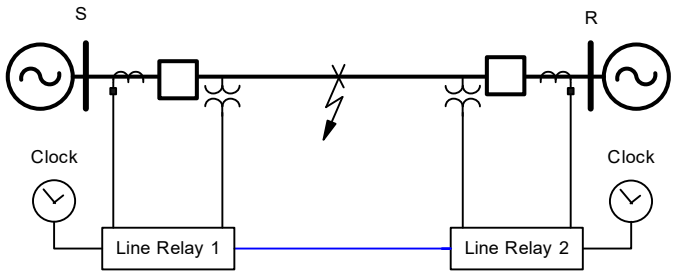

Fig. 4. Two-source power system with line relays exchanging voltage and current signals.

Fig. 5 shows phasor magnitudes for an internal A-phase-to-ground fault. Fig. 5 also shows a disturbance detector (DD) binary signal in the bottommost subplot. Assertion of a DD is used to identify the fault initiation time (T_{FAULT_INIT}). Using the fault initiation time as reference, the pre-fault data window (PreFltWin) and faulted data window (FltWin) are identified. The start time for FltWin depends on the phasor filter used in the relay. The start time is delayed until the phasor filter can estimate faulted phasors accurately. A short time-offset is applied to the PreFltWin to account for the delay in assertion of the DD. The width of the PreFltWin and FltWin are fixed independently [16]. The phasors in the PreFltWin and FltWin windows are used to calculate pre-fault phasors and faulted phasors for the proposed algorithm. Next, we discuss the proposed estimation method in detail.

A. *Pre-Fault Sequence Quantities*

Using sequence quantities in the pre-fault window (PreFltWin), pre-fault sequence quantities are calculated by taking an average, as shown in (6) and (7). If the maximum or minimum sequence quantity is significantly higher or lower than the average value, then the pre-fault sequence quantities are forced to zero (not used). This is to ensure that the power system is in steady state before the fault.

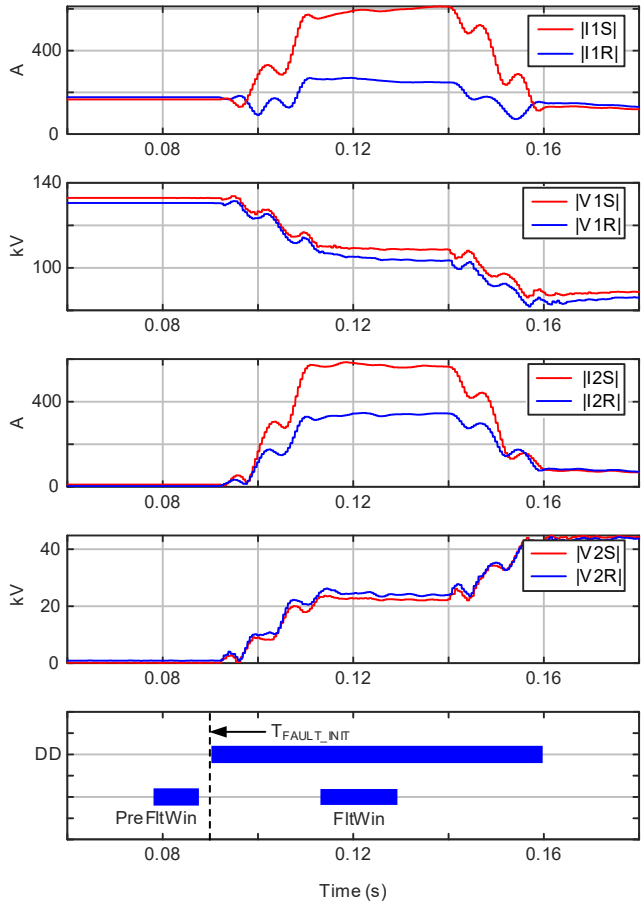

Fig. 5. Relay event showing fault initiation time, pre-fault data window, and faulted data window.

$$
\begin{aligned}
V_{1S\_PRE\text{-}FAULT} &= \text{avg}\,(V_{1S} \text{ in PreFltWin}) \\
I_{1S\_PRE\text{-}FAULT} &= \text{avg}\,(I_{1S} \text{ in PreFltWin}) \\
V_{2S\_PRE\text{-}FAULT} &= \text{avg}\,(V_{2S} \text{ in PreFltWin}) \\
I_{2S\_PRE\text{-}FAULT} &= \text{avg}\,(I_{2S} \text{ in PreFltWin})
\end{aligned} \tag{6}
$$

$$
\begin{aligned}
V_{1R\_PRE\text{-}FAULT} &= \text{avg}\,(V_{1R} \text{ in PreFltWin}) \\
I_{1R\_PRE\text{-}FAULT} &= \text{avg}\,(I_{1R} \text{ in PreFltWin}) \\
V_{2R\_PRE\text{-}FAULT} &= \text{avg}\,(V_{2R} \text{ in PreFltWin}) \\
I_{2R\_PRE\text{-}FAULT} &= \text{avg}\,(I_{2R} \text{ in PreFltWin})
\end{aligned} \tag{7}
$$

B. *Incremental Sequence Quantities*

Incremental sequence quantities (Δ) for pure-fault networks are calculated by subtracting averaged pre-fault sequence quantities calculated earlier from sequence quantities in the faulted window (FltWin), as shown in (8) and (9).

$$
\begin{aligned}
\Delta V_{1S} &= V_{1S\_FAULTED} - V_{1S\_PRE\text{-}FAULT} \\
\Delta I_{1S} &= I_{1S\_FAULTED} - I_{1S\_PRE\text{-}FAULT} \\
\Delta V_{2S} &= V_{2S\_FAULTED} - V_{2S\_PRE\text{-}FAULT} \\
\Delta I_{2S} &= I_{2S\_FAULTED} - I_{2S\_PRE\text{-}FAULT}
\end{aligned} \tag{8}
$$

$$
\begin{aligned}
\Delta V_{1R} &= V_{1R\_FAULTED} - V_{1R\_PRE\text{-}FAULT} \\
\Delta I_{1R} &= I_{1R\_FAULTED} - I_{1R\_PRE\text{-}FAULT} \\
\Delta V_{2R} &= V_{2R\_FAULTED} - V_{2R\_PRE\text{-}FAULT} \\
\Delta I_{2R} &= I_{2R\_FAULTED} - I_{2R\_PRE\text{-}FAULT}
\end{aligned} \tag{9}
$$

C. *Fault Location Estimation*

For unbalanced faults, fault location ($M_{UNBALANCED\_FAULT}$) is estimated by solving a negative-sequence pure-fault network (Fig. 6) using incremental negative-sequence quantities. Equation (10) is used to estimate fault locations for an unbalanced fault for all data points in the faulted window. Next, maximum and minimum estimates are discarded, and an average of the remaining estimates is the estimated fault location for the given fault.

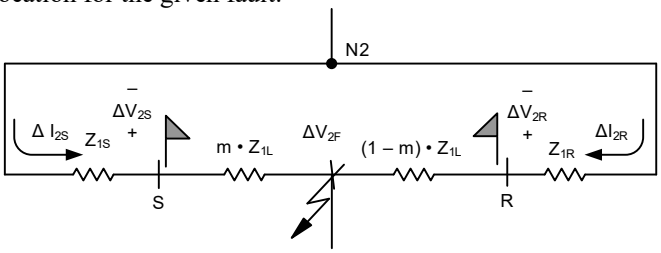

Fig. 6. Equivalent negative-sequence pure-fault network.

$$
m_{UNBALANCED\_FAULT} = \text{real}\left(\frac{\Delta V_{2S} - \Delta V_{2R} + Z_{1L} \bullet \Delta I_{2R}}{Z_{1L} \bullet \left(\Delta I_{2S} + \Delta I_{2R} \right)} \right) \tag{10}
$$

Fig. 7 shows the positive-sequence pure-fault network. For balanced faults, fault location ($M_{BALANCED\_FAULT}$) is estimated by solving a positive-sequence pure-fault network using equation (11). Maximum and minimum estimates are discarded, and an average of the remaining estimates is the fault location (m) estimate for the given fault.

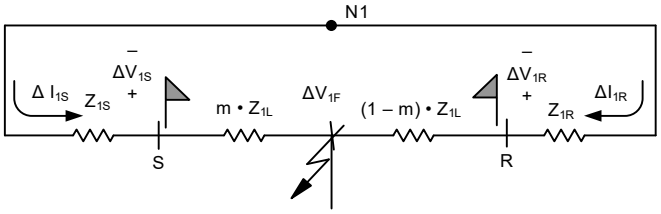

Fig. 7. Equivalent positive-sequence pure-fault network.

$$
m_{BALANCED\_FAULT} = \text{real}\left(\frac{\Delta V_{1S} - \Delta V_{1R} + Z_{1L} \bullet \Delta I_{1R}}{Z_{1L} \bullet \left(\Delta I_{1S} + \Delta I_{1R} \right)} \right) \tag{11}
$$

D. *Factors That Influence Fault Location Accuracy*

Voltage and current measurements in relays are impacted by inaccuracies in current transformers (CTs), potential transformers (PTs), and relay measurement circuits. Measurement errors have a direct impact on fault location

accuracy. Positive-sequence impedance (Z_{1L}) is used for fault location estimation for all fault types. Any error on the Z_{1L} value impacts fault location accuracy. The proposed method requires time-synchronized voltage and current samples from all remote terminals. Any issue with time-synchronization will result in a phase shift between local and remote signals, resulting in a fault location estimation error.

Evolving faults, CT saturation, coupling capacitor voltage transformers (CCVT) transients, faults with time-varying fault resistance, and fast breaker operation impact the accuracy of sequence quantities estimated by the relay in a faulted network. Errors in incremental sequence quantities impact the accuracy of fault location estimates. With untransposed lines, sequence networks are no longer independent. One sequence current flowing in an unbalanced system produces voltage drops in all three sequence networks [12]. The proposed method only subtracts the sequence quantities from the pre-fault network; however, it does not account for the coupling between sequence quantities in the pure-fault networks. The coupling of sequence quantities in the pure-fault network affects fault location accuracy.

VI. Simulation Results

To test the efficacy of the proposed method, simulations are executed and fault locations are estimated. For the single-circuit and double-circuit models shown in the Appendix, electromagnetic transient (EMT) simulations are run and event reports from both local and remote relays are captured. Each event report includes time-synchronized voltage and current signals from both ends of the line. For a three-terminal line, a phasor-based offline simulation is carried out. In the following subsections, each simulation result is discussed in detail.

A. Single-Circuit Untransposed Line (EMT Simulation)

An untransposed 400 kV single-circuit transmission line is modeled in the real-time digital simulator along with ac sources, CTs, CCVTs, and two-cycle circuit breakers. Line and source parameters are provided in the Appendix. The line length is set to100 km. Two line relays are connected to the secondary of the CT and CCVT and are configured to protect the line. Communication links between the two relays allow each relay to receive voltage and current signals from the other end. When any internal fault occurs on the line, both relays issue trip signals and isolate the fault. Following a fault, both relays store an event report. The event report contains time-synchronized voltage and current signals from both terminals and other information like fault type and DD. For fault location estimation using the proposed method, we use the event reports generated by the line relay at Terminal S.

At the fault location of 30 km from Terminal S, a total of 90 faults are simulated by varying load angle, fault resistance, and fault type in a nested loop, as shown below.

- Load angle (δ): 20°, 1°, –20°
  - Fault resistance (R_f): 0, 10, 20 ohms
    - Fault type: AG, BG, CG, AB, BC, CA, ABG, BCG, CAG, ABC

For these 90 faults, fault location is estimated by solving both the faulted network and the pure-fault network. For a faulted network, equations (3) and (4) are used, depending upon the fault type. Similarly, equations (10) and (11) are used for the proposed fault location method that solves pure-fault networks.

Fig. 8 shows the fault location estimates from both methods for the fault combinations discussed earlier. The top plot depicts the 30 fault location estimates for load angle (δ) of 20° by varying fault resistance and fault types. The first ten data points on the top plot correspond to fault location estimates for ten different fault types at $R_f = 0$. Data points 11 through 20 on the top plot correspond to fault location estimates for 10 different fault types at $R_f = 10$ ohms. Finally, data points 21 through 30 correspond to fault location estimates for 10 different fault types at $R_f = 20$ ohms. Similarly, the middle and bottom plots show the fault location estimates for load angle (δ) at 1° and –20° respectively. As discussed in Section III, at a high load angle, untransposed lines create both negative- and zero-sequence voltages and currents in the pre-fault network. This unbalance is responsible for poor fault location estimates when the faulted-network method is used. The proposed pure-fault network method subtracts pre-fault unbalance by solving a pure-fault network rather than a faulted network. As a result, the impact of pre-fault unbalance due to untransposed lines on fault location accuracy is minimized.

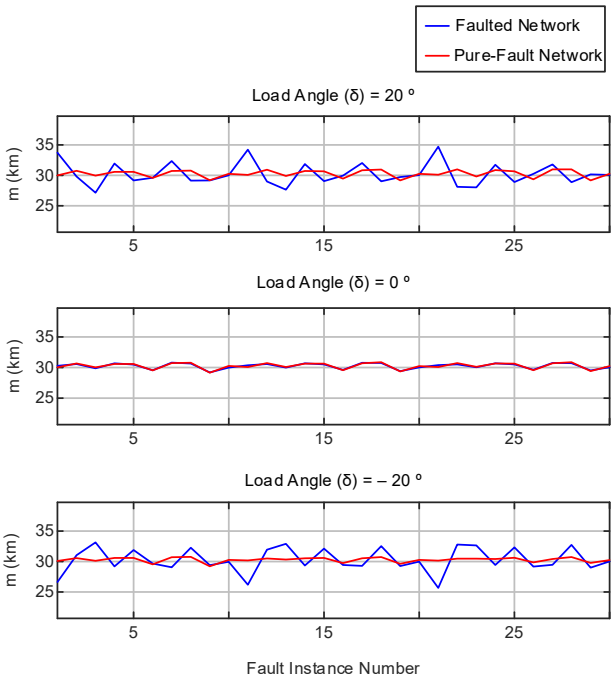

Fig. 8. Fault location estimates using faulted network and pure-fault network (proposed) for faults at 30 km on an untransposed single-circuit line.

The worst-case fault location absolute error and relative error based on line length [2] for both methods are shown in Table I.

TABLE I
WORST-CASE FAULT LOCATION ERROR FOR SINGLE-CIRCUIT LINE

	Faulted-Network Method		Pure-Fault Network Method (Proposed)	
Fault Location (km)	**Absolute Error (km)**	**Relative Error (%)**	**Absolute Error (km)**	**Relative Error (%)**
30	4.72	4.72	0.99	0.99

B. Double-Circuit Untransposed Lines (EMT Simulation)

For this test case, the single-circuit line from the previous power system model is replaced with an untransposed double-circuit line configuration. Line parameters and tower configuration for the double-circuit line are shown in the Appendix. A fault location of 30 km from Terminal S is selected and the same 90 faults are applied on the line.

Fig. 9 shows the fault location estimates using the faulted and pure-fault networks. Similar to the single-circuit line, the proposed method provides better fault location accuracy.

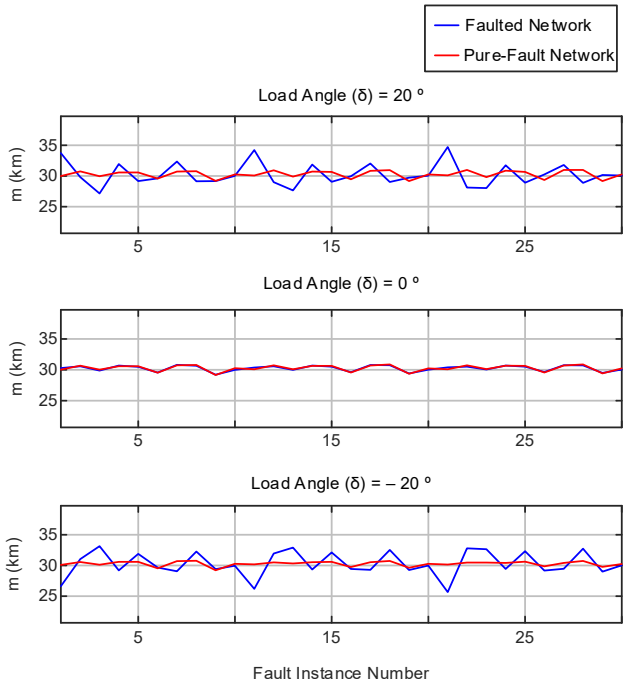

Fig. 9. Fault location estimates using faulted network and pure-fault network (proposed) for faults at 30 km on an untransposed double-circuit line.

The worst-case fault location absolute error and relative error based on line length for the case of a double-circuit line are shown in Table II.

TABLE II
WORST-CASE FAULT LOCATION ERROR FOR DOUBLE-CIRCUIT LINE

	Faulted-Network Method		Pure-Fault Network Method (Proposed)	
Fault Location (km)	**Absolute Error (km)**	**Relative Error (%)**	**Absolute Error (km)**	**Relative Error (%)**
30	8.25	8.25	0.49	0.49

C. Three-Terminal Untransposed Lines (Phasor-Based Offline Simulation)

The line configuration and source parameters for a three-terminal line is shown in the Appendix. The 400 kV three-terminal untransposed line is modeled in a phasor-based offline simulation tool. Similar to the previous case, 90 faults are applied at the fault location of 30 km from Terminal S. Because of the phasor-based simulation, only one data point is available for faulted and pre-fault networks. Pure-fault sequence quantities are computed for all three terminals by subtracting pre-fault sequence quantities from the faulted sequence quantities.

The method described in [7] is used to identify the faulted line segment and then reduce three-terminal line arrangements into a two-terminal equivalent. For faults on Line Segment 1, the tap point becomes the remote terminal for Terminal S. Once the equivalent two-terminal network is developed, the pure-fault network is further developed.

Fault location estimates from both methods are shown in Fig. 10. The faulted-network-based method has significant fault location error for high load angles. The proposed method improves the fault location accuracy significantly for the case of three-terminal lines.

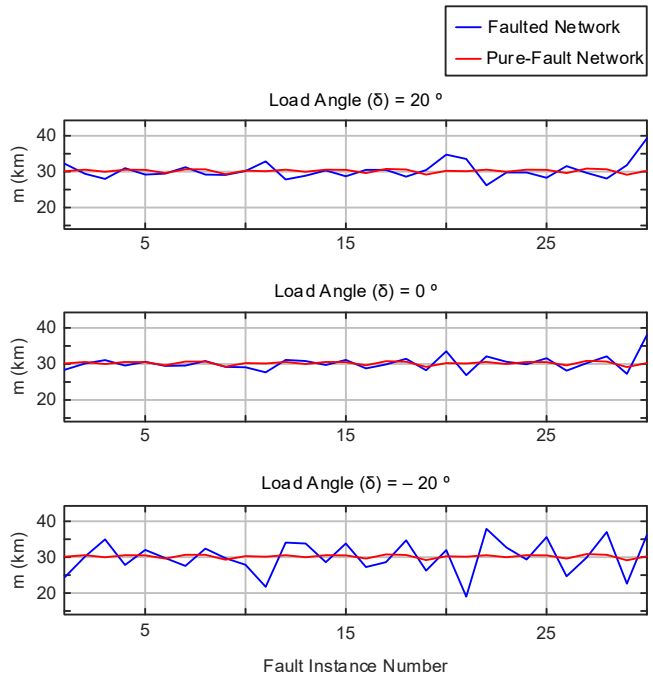

Fig. 10. Fault location estimates using faulted network and pure-fault network (proposed) for faults at 30 km from Terminal S on an untransposed three-terminal line.

The worst-case fault location absolute error and relative error based on line length for both methods are shown in Table III. Note that the error for the proposed method is very small. This is because the results are based on offline phasor-based simulations. Unlike in EMT simulation, errors associated with time-domain dynamic simulation, data acquisition, and other measurement errors are not present.

TABLE III
WORST-CASE FAULT LOCATION ERROR FOR THREE-TERMINAL LINE

	Faulted-Network Method		Pure-Fault Network Method (Proposed)	
Fault Location (km)	**Absolute Error (km)**	**Relative Error (%)**	**Absolute Error (km)**	**Relative Error (%)**
30	11	11	0.88	0.88

VII. FIELD RESULTS

Field records are used to test the effectiveness of the proposed fault location method. Although we extensively tested the proposed method with EMT simulations, the field results provided additional validation for the proposed method. For these tests, we used time-synchronized event records from traveling-wave relays installed in the field. Using event records, fault locations are estimated using the faulted-network method and proposed pure-fault method for three field events. Table IV provides information on fault location reported by the utility, double-ended traveling-wave-based fault location provided by traveling-wave relays, and fault location estimates using the faulted-network and proposed pure-fault network methods. In each case, the traveling-wave relay estimated fault locations were very close to the actual fault location. Table IV also provides additional information such as line voltage level, line length, unbalance in pre-fault network (|I2|/|I1|), load angle, and fault type.

Event 1 in Table IV is associated with a BG fault that occurred at 33.86 km from one end of a transmission line in Spain. The line of interest is 61.98 km long and its operating voltage is 220 kV. The fault location estimated by the traveling-wave relay, proposed pure-fault network method, and faulted-network methods are 33.84 km, 34.1 km, and 34.26 km respectively. For this event, the pre-fault unbalance (|I2|/|I1|) is low at 1.54 percent. As discussed in previous sections, with low pre-fault unbalance, the fault location accuracy provided by the proposed method approaches close to the faulted-network method. The TWFL is very close to the actual fault location. Between two phasor-based methods, the proposed method has an error of 0.24 km, as compared to 0.4 km error provided by the faulted-network method.

Event 2 in Table IV comes from a 230 kV, 153.16 km long two-terminal line from Columbia. The event was captured during an internal CG fault at 61.5 km from one end of the line. The pre-fault unbalance for the transmission line is 6.94 percent. For this event, the proposed pure-fault network estimated the fault location of 60.93 km, whereas the faulted-network method estimated the fault location 63.1 km. The fault location errors for the two methods are 0.58 km and 1.59 km, respectively. If we assume one tower spans 300 m, the proposed method provided a fault location estimate within two tower spans, whereas the faulted-network method estimated within five tower spans.

Event 3 in Table IV is associated with an AG internal fault on a 132 kV, 107.23 km long transmission line in India. The fault occurred at 101.33 km from one end of the line. The pre-fault unbalance prior to the fault is 12.76 percent. Fig. 11 shows local and remote terminal voltages and currents obtained from the remote terminal relay during the fault. For the same event, Fig. 12 shows the sequence quantities, pre-fault window, fault initiation time, and faulted window. The pre-fault |V2S| in the pre-fault window is around 8.15 percent of faulted |V2S|. The pre-fault unbalance is high for this event. The fault location estimated by the traveling-wave relay, proposed pure-fault network method, and faulted-network methods are 101.27 km, 100.49 km, and 104.01 km, respectively. For this event with a high pre-fault unbalance, the proposed method fault location accuracy is three times better than the faulted-network method.

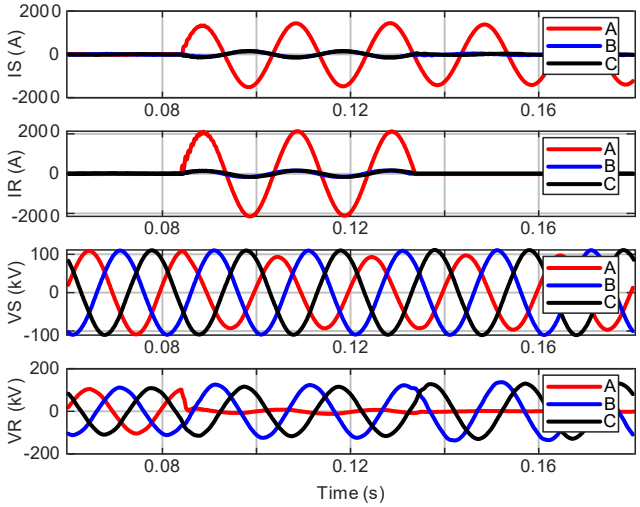

Fig. 11. Local and remote terminal voltages and currents for Event 3.

TABLE IV
MULTI-ENDED FAULT LOCATION ESTIMATION USING FIELD EVENT REPORTS

Event #	Line Voltage (kV)	Line Length (km)	|I2_Prefault|/ |I1_Prefault| %	Fault Type	Actual Fault Location (km)	TWFL Method [Fault Location-km, error-km]	Pure-Fault Network Method [Fault Location-km, error-km]	Faulted-Network Method [Fault Location-km, error-km]
1	220	61.98	1.54	BG	33.86	[33.87, 0.01]	[34.1, 0.24]	[34.26, 0.40]
2	230	153.16	6.94	CG	61.50	[60.99, 0.51]	[60.93, 0.57]	[63.1, 1.6]
3	132	107.23	12.76	AG	101.33	[101.27, 0.06]	[100.49, 0.84]	[104.01, 2.68]

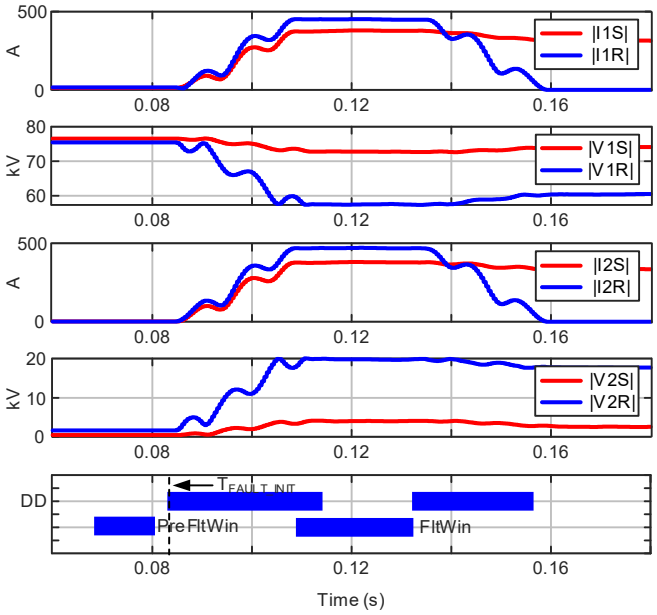

Fig. 12. Local and remote sequence quantities for Event 3. The bottom plot shows the pre-fault and faulted window selected by the proposed method.

For the three events discussed in this section, traveling-wave relays provided the most accurate fault locations. These field results prove the superiority of traveling-wave-based fault location method. Between the two phasor-based multi-ended fault location methods, the proposed pure-fault network method provides much more accurate fault location estimates than the traditional faulted-network method. Improvement in fault location accuracy increases when there is a high pre-fault unbalance. The fault location accuracy of the proposed method falls between the traveling-wave and faulted-network methods.

VIII. Conclusion

Following a fault in the transmission line, access to accurate fault locations assists utility crews to quickly make necessary repairs and restore service. Traveling-wave-based fault location methods are superior, however, not all relays have the capability to apply traveling-wave algorithms. This paper describes a new multi-ended fault location algorithm using pure-fault networks and incremental sequence quantities. The proposed method uses time-synchronized voltage and current samples from all remote terminals, which makes it suitable for integration in line current differential relays. The proposed method is rigorously tested using both EMT simulations and field events. Compared to the traditional faulted-network method, the proposed pure-fault method provides accurate fault location estimates when an unbalance exists in a pre-fault state. Untransposed lines with heavy load flow and unbalanced loads create unbalance in the power system. Because the proposed method uses incremental quantities, it removes the impact of pre-fault unbalance and improved fault location accuracy.

IX. Appendix

The parameters for the 400 kV overhead transmission line are listed in Table V and Table VI.

Table V
Line Parameters for a 400 kV Single-Circuit Overhead Line

Line Parameters	Values
Phase conductor outside diameter	3.177 cm
Phase conductor thickness/diameter ratio (T/D)	0.5
Phase conductor dc resistance	0.0547 Ω/km
Number of bundled conductors per phase	4
Shield conductor outside diameter	0.824 cm
Shield conductor thickness/diameter ratio (T/D)	0.5
Shield conductor dc resistance	0.8525 Ω/km
Number of bundled conductors per shield	1
Horizontal tower configuration (A–B–C–Shield1–Shield2)	(0–11–22–2.97–19.03) m
Vertical tower configuration (A–B–C–Shield1–Shield2)	(21.798–21.798–21.798–29.27–29.27) m
Vertical mid-span configuration (A–B–C–Shield1–Shield2)	(8.84–8.84–8.84–17.27–17.27) m
Soil resistivity	100 Ω-m
Line length	100 km

For the given line, RLC matrices at 60 Hz are listed in (12).

$$R_{matrix}\left(\frac{\Omega}{km}\right)=\begin{bmatrix}0.11208 & 0.09848 & 0.09458\\ 0.09848 & 0.11504 & 0.09848\\ 0.09458 & 0.09848 & 0.11208\end{bmatrix}$$
$$L_{matrix}\left(\frac{H}{km}\right)=\begin{bmatrix}0.00139 & 0.00053 & 0.00041\\ 0.00053 & 0.00137 & 0.00053\\ 0.00041 & 0.00053 & 0.00139\end{bmatrix} \quad (12)$$
$$C_{matrix}\left(\frac{nF}{km}\right)=\begin{bmatrix}11.7781 & -1.71828 & -0.417076\\ -1.71828 & 12.0501 & -1.71826\\ -0.417076 & -1.71826 & 11.7781\end{bmatrix}$$

Positive-sequence and zero-sequence parameters at 60 Hz are listed in (13).

$$[R1,R0](\Omega/km)=[0.01589 \quad 0.30742]$$
$$[L1,L0](H/km)=[0.00090 \quad 0.00237] \quad (13)$$
$$[C1,C0](nF/km)=[13.1533 \quad 9.29971]$$

The two-source power system model with a single-circuit line used for EMT simulation to test the proposed multi-ended impedance fault location estimation algorithm is shown in Fig. 1.

The transmission line Z_{1L} and Z_{0L} parameters are provided in (13). The source impedances are shown in (14).

$$Z_{1S}=1.0\bullet|Z_{1L}|\angle 82.3°$$
$$Z_{0S}=1.0\bullet|Z_{0L}|\angle 66.9° \quad (14)$$
$$Z_{1R}=1.5\bullet|Z_{1L}|\angle 82.3°$$
$$Z_{0R}=1.5\bullet|Z_{0L}|\angle 66.9°$$

TABLE VI
LINE PARAMETERS FOR A 400 KV DOUBLE-CIRCUIT OVERHEAD LINE

Line Parameter	Values
Phase conductor outside diameter	3.177 cm
Phase conductor thickness/diameter ratio (T/D)	0.5
Phase conductor dc resistance	0.0547 Ω/km
Number of conductors per bundle	4
Shield conductor outside diameter	0.824 cm
Shield conductor thickness/diameter ratio (T/D)	0.5
Shield conductor dc resistance	0.85252 Ω/km
Number of conductors per bundle	1
Horizontal tower configuration (A1–B1–C1–A2–B2–C2–Shield1–Shield2)	(0–0.6–2.22–15–14.4–12.78–4.0996–10.8997) m
Vertical tower configuration (A1–B1–C1–A2–B2–C2–Shield1–Shield2)	(28.2002–36.2001–44.2001–28.2002–36.2001–44.2001–60.0002–60.0002) m
Vertical mid-span configuration (A1–B1–C1–A2–B2–C2–Shield1–Shield2)	(18.8001–24.1341–29.4682–18.8001–24.1341–29.4682–40.0001–40.0001) m
Soil resistivity	100 Ω-m
Line length	100 km

For the given line, RLC matrices at 60 Hz are listed in (15).

$$\begin{bmatrix} 0.09102 & 0.07937 & 0.08312 & 0.07676 & 0.07931 & 0.08304 \\ 0.07937 & 0.09648 & 0.08649 & 0.07931 & 0.08218 & 0.08636 \\ 0.08312 & 0.08649 & 0.10556 & 0.08304 & 0.08636 & 0.09118 \\ 0.07676 & 0.07931 & 0.08304 & 0.09102 & 0.07937 & 0.08312 \\ 0.07931 & 0.08218 & 0.08636 & 0.07937 & 0.09648 & 0.08648 \\ 0.08304 & 0.08636 & 0.09118 & 0.08312 & 0.08648 & 0.10556 \end{bmatrix}$$

$$L_{MATRIX}\left(\frac{H}{km}\right)$$

$$= \begin{bmatrix} 0.00149 & 0.00074 & 0.00058 & 0.00058 & 0.00056 & 0.00051 \\ 0.00074 & 0.00146 & 0.00069 & 0.00056 & 0.00056 & 0.00054 \\ 0.08312 & 0.00069 & 0.00141 & 0.00051 & 0.00054 & 0.00057 \\ 0.00058 & 0.00056 & 0.00051 & 0.00149 & 0.00074 & 0.00058 \\ 0.00056 & 0.00056 & 0.00054 & 0.00074 & 0.00146 & 0.00069 \\ 0.00051 & 0.00054 & 0.00057 & 0.00058 & 0.00069 & 0.00141 \end{bmatrix}$$

$$C_{MATRIX}\left(\frac{nF}{km}\right) =$$

$$\begin{bmatrix} 012.00540 & -3.238190 & -1.084030 & -1.018000 & -0.727254 & -0.526826 \\ -3.238190 & 012.67480 & -3.113830 & -0.727254 & -0.849590 & -0.913725 \\ -1.084030 & -3.113830 & 012.09310 & -0.526826 & -0.913725 & -1.765400 \\ -1.018000 & -0.727254 & -0.526826 & 012.00540 & -3.238200 & -1.08404 \\ -0.727254 & -0.849590 & -0.913725 & -3.238200 & 012.67480 & -3.11384 \\ -0.526826 & -0.913725 & -1.765400 & -1.084040 & -3.113830 & -12.0931 \end{bmatrix} \quad (15)$$

Positive-, zero-, and mutual zero-sequence parameters of Circuit-1 and Circuit-2 at 60 Hz are listed in (16).

$$\begin{aligned} &\left[R1(1), R0(1), R0_{MUTUAL}, R1(2), R0(2)\right]\left(\frac{\Omega}{km}\right) \\ &= \left[0.01469 \quad 0.26367 \quad 0.24918 \quad 0.01469 \quad 0.26367\right] \\ &\left[L1(1), L0(1), L0_{MUTUAL}, L1(2), L0(2)\right]\left(\frac{H}{km}\right) \\ &= \left[0.00079 \quad 0.00280 \quad 0.00164 \quad 0.00079 \quad 0.00280\right] \\ &\left[C1(1), C0(1), C0_{MUTUAL}, C1(2), C0(2)\right]\left(\frac{nF}{km}\right) \\ &= \left[0.147365 \quad 7.3004 - 2.65619 \quad 0.147365 \quad 7.30038\right] \end{aligned} \quad (16)$$

The two-source power system model with a double-circuit line used for EMT simulation to test the proposed multi-ended impedance fault location estimation algorithm is shown in Fig. 13.

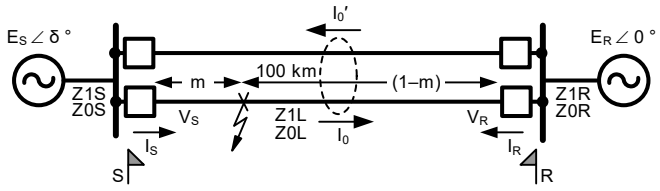

Fig. 13. Two-source power system model with double-circuit line.

The transmission line Z_{1L} and Z_{0L} parameters are provided in (16). The source impedances are shown in (17).

$$\begin{aligned} Z_{1S} &= 1.0 \bullet \left|Z_{1L}\right| \angle 82.3° \\ Z_{0S} &= 1.0 \bullet \left|Z_{0L}\right| \angle 66.9° \\ Z_{1R} &= 1.5 \bullet \left|Z_{1L}\right| \angle 82.3° \\ Z_{0R} &= 1.5 \bullet \left|Z_{0L}\right| \angle 66.9° \end{aligned} \quad (17)$$

The three-source power system model used for phasor simulation to test the proposed multi-ended impedance fault location estimation is shown in Fig. 14.

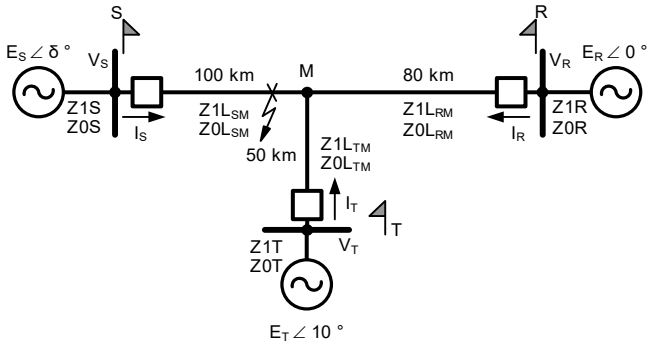

Fig. 14. Three-source power system model.

The transmission line Z_{1L} and Z_{0L} parameters are provided in (13). The source impedances are shown in (18).

$$\begin{aligned} Z_{1S} &= 0.1 \bullet \left|Z_{1L\_SM}\right| \angle 82.3° \\ Z_{0S} &= 0.1 \bullet \left|Z_{0L\_SM}\right| \angle 66.9° \\ Z_{1R} &= 0.15 \bullet \left|Z_{1L\_RM}\right| \angle 82.3° \\ Z_{0R} &= 0.15 \bullet \left|Z_{0L\_RM}\right| \angle 66.9° \\ Z_{1T} &= 0.2 \left|Z_{1L\_TM}\right| \angle 77.32° \\ Z_{0T} &= 0.2 \bullet \left|Z_{0L\_TM}\right| \angle 61.98° \end{aligned} \quad (18)$$

X. References

[1] G. Benmouyal and J. Roberts, "Superimposed Quantities: Their True Nature and Application in Relays," proceedings of the 26th Annual Western Protective Relay Conference, Spokane, WA, October 1999.

[2] IEEE Std C37.114-2014, *IEEE Guide for Determining Fault Location on AC Transmission and Distribution Lines*.

[3] S. Marx, B. Johnson, A. Guzmán, V. Skendzic, and V. Mynam, "Traveling Wave Fault Location in Protective Relays: Design, Testing, and Results," proceedings of the 16th Annual Georgia Tech Fault and Disturbance Analysis Conference, Atlanta, GA, May 2013.

[4] E. O. Schweitzer, A. Guzmán, M. V. Mynam, V. Skendzic, B. Kasztenny, and S. Marx, "Locating faults by the traveling waves they launch," 2014 67th Annual Conference for Protective Relay Engineers, College Station, TX, USA, 2014, pp. 95-110, doi: 10.1109/CPRE.2014.6798997.

[5] D. Córton, J. Melado, J. Cruz, R. Kirby, Y. Korkmaz, G. Patti, and G. Smelich, "Double-Ended Traveling-Wave Fault Locating Without Relay-to-Relay Communications," proceedings of the 74th Annual Conference for Protective Relay Engineers, Virtual Format, March 2021.

[6] H. Prado-Félix, V. Serna-Reyna, V. Mynam, M. Donolo, and A. Guzmán, "Improve Transmission Fault Location and Distance Protection Using Accurate Line Parameters," proceedings of the 40th Annual Western Protective Relay Conference, Spokane, WA, October 2013.

[7] D. Tziouvaras, J. Roberts, and G. Benmouyal, "New Multi-Ended Fault Location Design for Two- or Three-Terminal Lines," proceedings of CIGRE Study Committee B5 Colloquium, Florence, Italy, October 1999.

[8] B. Kasztenny, B. Le, and N. Fischer, "A New Multiterminal Fault Location Algorithm Embedded in Line Current Differential Relays," proceedings of the 11th Annual International Conference on Development in Power System Protection, Birmingham, United Kingdom, April 2012.

[9] Power System Relay Committee, Working Group D6, "AC Transmission Line Model Parameter Validation," IEEE Power and Energy Society, September 2014.

[10] Y. Xue, D. Finney, and B. Le, "Charging Current in Long Lines and High-Voltage Cables – Protection Application Considerations," proceedings of the 39th Annual Western Protective Relay Conference, Spokane, WA, October 2012.

[11] D. C. Deloach, J. D. Kuhlers, A. M. Murphy, and G. E. Piercy, "Voltage Unbalance in a Changing Grid," proceedings of the Annual Georgia Tech Fault and Disturbance Analysis Conference, Atlanta, GA, May 2022.

[12] J. Blackburn and T. Domin, Protective Relaying: Principles and Applications (Third Edition), CRC Press, Boca Raton, FL, 2006.

[13] E. O. Schweitzer, B. Kasztenny, A. Guzmán, V. Skendzic, and V. Mynam, "Speed of Line Protection – Can We Break Free of Phasor Limitations?" proceedings of the 68th Annual Conference for Protective Relay Engineers, College Station, TX, March 2015.

[14] B. Kasztenny, A. Guzmán, N. Fischer, V. Mynam, and D. Taylor, "Practical Settings Considerations for Protective Relays That Use Incremental Quantities and Traveling Waves," proceedings of the 43rd Annual Western Protective Relay Conference, Spokane, WA, October 2016.

[15] B. Kasztenny, G. Benmouyal, H. J. Altuve, and N. Fischer, "Tutorial on Operating Characteristics of Microprocessor-Based Multiterminal Line Current Differential Relays," proceedings of the 38th Annual Western Protective Relay Conference, Spokane, WA, October 2011.

[16] A. Shrestha and S. K. Mutha, "Transmission Line Parameter Estimation Using Traveling-Wave Fault Location Data," proceedings of the 75th Annual Conference for Protective Relay Engineers, College Station, TX, March 2022.

XI. Biographies

Arun Shrestha received his BSEE from the Institute of Engineering, Tribhuvan University, Nepal, in 2005, and his MS and PhD in electrical engineering from the University of North Carolina at Charlotte in 2009 and 2016, respectively. He joined Schweitzer Engineering Laboratories, Inc. (SEL) in 2011 as an associate power engineer in research and development. He is presently working as a senior engineer. His research areas of interest include power system protection and control design, real-time power system modeling and simulation, wide-area protection and control, power system stability, and digital substations. He is a senior member of IEEE and is a registered Professional Engineer. He is a member of IEEE PSRC and a U.S. representative to IEC 61850 TC 57 WG 10.

Sathish Kumar Mutha received his bachelor's degree in electrical and electronics engineering from Adam's engineering college, Paloncha, India, in 2008 and his MS degree in electrical engineering in 2020 from the University of North Carolina at Charlotte. Prior to earning his MS degree, he worked for over nine years as a coal-based power plant operations engineer at Heavy Water Board, Dept of Atomic Energy, India. He joined Schweitzer Engineering Laboratories, Inc. (SEL) in 2019 as an engineer intern and currently holds a position of power engineer in research and development division.